Wide structural and magnetic successive transitions and related magnetocaloric properties in a directionally solidified polycrystalline Ni-Co-Mn-In alloy

F. Chen[a, *], J. L. Sánchez Llamazares[b,], C. F. Sánchez-Valdés[c], P. Müllner[d], Y. X. Tong[a], L. Li[a]**

[a] Institute of Materials Processing and Intelligent Manufacturing, College of Materials Science and Chemical Engineering, Harbin Engineering University, Harbin, 150001, China.

[b] Instituto Potosino de Investigación Científica y Tecnológica A.C., Camino a la Presa San José 2055, Col. Lomas 4ª sección, San Luis Potosí, S.L.P. 78216, México

[c] División Multidisciplinaria, Ciudad Universitaria, Universidad Autónoma de Ciudad Juárez (UACJ), calle José de Jesús Macías Delgado # 18100, Ciudad Juárez, Chihuahua, México.

[d] Micron School of Materials Science and Engineering, Boise State University, ID 83725, USA.

*chenfeng01@hrbeu.edu.cn, **jose.sanchez@ipicyt.edu.mx

Abstract

We fabricated a $Ni_{45}Co_{6.4}Mn_{37}In_{11.6}$ polycrystalline sample with a specific texture using the directional solidification method. The structural and magnetic transitions as well as the related magnetocaloric effects were studied. This material exhibits wide structural and magnetic successive phase transitions. For both transitions, applying a magnetic field considerable extends the temperature intervals. For a magnetic field change of 5 T, the total working temperature window is up to 118 K. Furthermore, because of the large temperature range, the refrigeration capacity reached high values of 118 and 95 Jkg^{-1} for the structural and magnetic transition, respectively.

Keywords: Ni-Co-Mn-In; magnetic shape memory alloy; magnetocaloric materials; structural and magnetic transitions; working temperature range.

1 Introduction

Ni-Co-Mn-In magnetic shape memory alloys have attracted much attention in the field of magnetic cooling technology for their considerable magnetocaloric properties [1-4]. For example, in a $Ni_{45}Mn_{37}In_{13}Co_5$ ribbon, the maximum magnetic entropy change ΔS_M^{peak} is up to 34 $J\cdot kg^{-1}\cdot K^{-1}$ for $\mu_o\Delta H$ = 5 T, which is among the largest reported ΔS_M^{peak} in Ni-Mn-based Heusler alloys [2].

In $Ni_{45.7}Mn_{36.6}In_{13.5}Co_{4.2}$ alloy, at a field change of $\mu_0\Delta H$ = 1.95 T, the adiabatic temperature change, ΔT_{ad} reaches a very high magnitude of -8 K after the first field application [5]. Subsequently a reversible ΔT_{ad} of -3 K can be obtained which is comparable to that of $La(Fe,Si,Co)_{13}$, an important magnetic refrigerants [5]. $Ni_{42}Co_8Mn_{37.7}In_{12.3}$ alloy possesses a giant refrigeration capacity *RC* of 549 $J\cdot K^{-1}$ under 6 T field. Such a *RC* is significantly larger than most of the reported in Ni-Mn-based Heusler alloys [6]. All the above mentioned parameters of magnetocaloric properties including ΔS_{max}, ΔT_{ad}, and *RC* occur near room temperature. This makes Ni-Co-Mn-In alloys attractive candidate materials for room-temperature magnetic cooling.

From a practical viewpoint, a magnetocaloric material must have a wide working temperature window. For Ericsson cycle based magnetic refrigeration, magnetocaloric materials should exhibit a constant magnetic entropy change (ΔS_M) over a wide temperature range [7]. The working temperature range is usually estimated as the full-width at half-maximum (δT_{FWHM}) of the thermal dependence of the magnetic entropy change curve $\Delta S_M(T)$. This means δT_{FWHM} should be large. Several research groups have proposed ways to extend the working temperature range of a given alloy by introducing successive magnetic transitions [8, 9] or a single broad structural transition [10]. Few works reported large δT_{FWHM} associated with the structural and magnetic successive transitions, which is the focus of our present work.

2 Experimental procedures

A $Ni_{45}Co_{6.4}Mn_{37}In_{11.6}$ polycrystalline sample was obtained from a directionally solidified rod. Ref. [10] presents the processing parameters. The microstructure was examined perpendicular to the growth direction using a LEO model 1430VP scanning electron microscope equipped with an energy dispersive X-ray spectroscopy (EDS) for measuring the chemical composition. The SEM image was taken in backscattering emission mode. XRD analysis was performed at room temperature using copper $K_{\alpha 1}$ radiation.

Magnetization characterization was performed by vibrating sample magnetometry in a Quantum Design PPMS® Dynacool® system. Measurements were performed on a needle-shaped sample with the approximate dimensions 0.8×0.8×4.0 mm^3 (cut from the produced ingot) directly glued with high temperature zyrcar cement to the VSM oven heater stick. The external magnetic field $\mu_o H$ was applied along the major axis of the sample that was parallel to the direction of solidification. The magnetization vs. temperature $M(T)$ curves were measured at a heating/cooling rate of 1.0 K/min. The magnetic entropy change (ΔS_M) as a function of temperature curves across the structural and magnetic transitions were calculated using the Maxwell relation from a set of isothermal magnetization curves $M(\mu_o H)$ measured from 320 to 600 K. To avoid the influences resulting from the sample history, the following thermal protocol was followed prior to measuring each $M(\mu_o H)$ curve: at zero magnetic field the sample was heated to 475 K to stabilize austenite, cooled to 300 K to completely transform into martensite, and then heated again in no-overshot mode to the selected measuring temperature.

3 Results and discussion

Fig. 1(a) is an XRD pattern taken at room temperature (293 K). Two characteristic peaks, (222) and (400) related to a tetragonal martensitic structure. This is one of three common martensitic structure (the other two are 14M with a monoclinic unit cell and 10 M with an orthorhombic unit cell) for Ni-Mn based Heusler alloys [11]. The lattice parameters were $a = b = 0.7834$ nm, $c = 0.6823$ nm, and $c/a = 0.87$. The missing of other reflections and considerably strong intensity of (222) and (400) peaks may suggest that the sample was strongly textured [12-14] and polycrystalline.

Commented [CU1]: In Ni-Mn-Ga, the c/a ratio for NM tetragonal martensite is larger than 1 if one uses the "cubic" axis system. What axis system did you use for indexing the peaks?

Fig. 1(b) shows a back-scattered electron (BSE) image. The microstructure consists of dual phase: grey matrix phase and dark second phase. The lath-like surface relief feature, combined with XRD result (as shown in Fig. 1(a)) indicates that the matrix phase was martensite. The image in Fig. 1(b) contains several martensite variants. Second phase particles with various sizes were

unevenly distributed in the matrix, most of which exhibited an approximately spherical shape. The actual composition was $Ni_{42.9}Co_{16.5}Mn_{39.1}In_{1.5}$ (determined with EDS) meaning that this second phase was Co-rich γ, which often forms in some Co-containing Ni-Mn-based Heusler alloys, such as the annealed $Ni_{46}Mn_{35}In_{14}Co_5$ ribbons [3] and $Ni_{37.7}Co_{12.7}Mn_{40.8}Sn_{8.8}$ ribbons [15], $Ni_{38}Co_{12}Mn_{41}Sn_9$ polycrystals [16], and $Ni_{42}Co_8Mn_{38}In_{12}$ polycrystals [10]. The γ-phase in Ni-Mn-based Heusler alloys (i) enhances the degree of chemical inhomogeneity [10] and adjust the composition of matrix [17], (ii) changes the martensitic transformation temperatures, (iii) weakens the magnetocaloric effects, MCE [3, 15], (iv) improves the mechanical properties [18], and (v) reduces the functional properties such as shape memory recovery and pseudoelastic behavior [18]. Here, we are mostly concerned with the first three effects. Due to the increasing fraction of second phase, the content of Sn in the matrix increases apparently for $Ni_{50}Mn_{40-x}Sn_{10}Fe_x$ (x = 0, 3, 4, 5, 6) alloys [17]. This is mainly resulted from the change of matrix composition. The value of ΔS_M is remarkably reduced by about 9.4 J kg^{-1} K^{-1} due to the formation of γ phase in $Ni_{46}Mn_{35}In_{14}Co_5$ ribbons [3]. The reason is that the second phase does not participate in the magnetostructural transition. The γ phase can reduce the general brittleness and increase the strength by preventing the propagation of cracks [18].

Commented [CU2]: How? Increases or decreases?

Commented [CU3]: In what sense? Does it increase ductility or toughness or strength or something else?

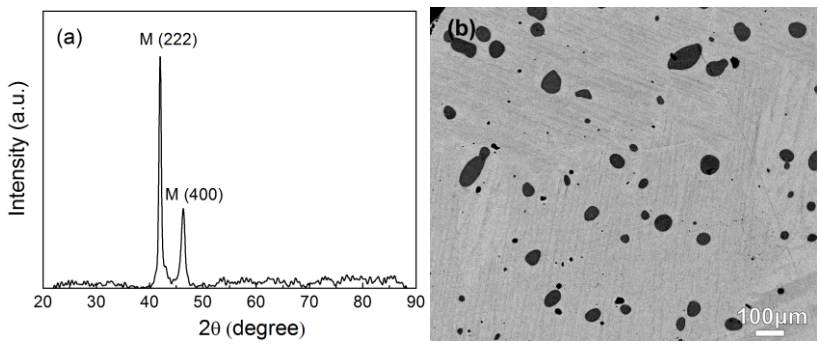

Fig. 1 (a) XRD pattern and (b) SEM image taken in backscattering emission mode.

Fig. 2 shows the magnetization vs. temperature *M*(*T*) curves measured under 5 mT and 5 T magnetic fields. In a magnetic field of 5 mT, the sample exhibited a broad first-order structural transition (ST) on heating starting at 371 K and finishing at 431 K, immediately followed by a second-order magnetic transition (MT). That is, the wide structural and magnetic successive transitions were realized for the present sample. Chemical heterogeneity introduced by chemical segregation through the Bridgman-Stockbarger method and enhanced by the precipitation of γ phase extended the temperature range for both ST and MT [10]. A magnetic field of 5 T shifted the starting and finishing temperatures of the ST upon heating towards 327 K and 418 K, respectively. Thus, the transition interval was extended from 60 to 91 K. The temperature interval for MT was also enlarged to 67 K (from 449 K to 516 K). Such wide temperature intervals for both the ST and MT suggest a large δT_{FWHM} can be achieved not only within the ST but also in the MT. Furthermore, the large $\delta T_{FWHM}$is leads to a greater *RC* value [8]. However, the magnetization difference between the austenite and martensite, $\Delta M_{A\text{-}M}$ is as low as 30.8 A m^2 kg^{-1} under 5 T field. Large $\Delta M_{A\text{-}M}$ values are required for a large driving force for inducing the structural transition unless applying a remarkably high magnetic field [19, 20].

Commented [CU4]: This value is not resolved in Fig. 2.

Commented [CU5]: It looks more like 465 K to me.

Commented [CU6]: This seems wrong. The magnetic transition occurs at one single temperature. It seems that Tc at 5 mT is about 445 K and at 5 T it is about 515 K.
What causes this large field dependence?

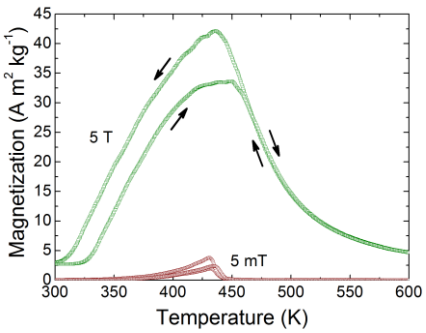

Fig. 2 Thermal dependence of magnetization, *M*(*T*) curves measured in ZFC and FC regimens under static magnetic fields of 5 mT and 5 T.

Fig. 3(a) and (b) show the isothermal magnetization versus magnetic field, $M(\mu_o H)$ curves around the reverse ST and MT, respectively. In Fig. 3(a), $M(\mu_o H)$ curves between 320 K and 431 K show a typical ferromagnetic behavior. In other words, no metamagnetic-like behaviour occured. As discussed above, this can be ascribed to the low $\Delta M_{A\text{-}M}$ (determined from Fig. 2) because the metamagnetic-like behavior is associated with the magnetic-field induced reverse ST. Metamagnetic-like magnetization behavior adds substantially to the giant MCE for Ni-Mn based Heusler alloys [3, 21-25], such as $Ni_{45}Co_5Mn_{36.6}In_{13.4}$ ($\Delta S_M^{peak} = 28.4$ J kg^{-1} K^{-1}) [21]. The ΔS_M^{peak} is 9.1 J kg^{-1} K^{-1} for $Ni_{50}Mn_{37}Sb_{13}$ and is larger than 5.2 J kg^{-1} K^{-1} for $Ni_{50}Mn_{36}Sb_{14}$ as the former exhibits a stronger metamagnetic-like feature than the latter [22]. Therefore, the absence of metamagnetic-like behavior for the present sample causes a small ΔS_M. During the magnetic transition as shown in Fig. 3(b), ferromagnetic behavior is observed between 431 and 479 K, as well as paramagnetic behavior is found between 485 and 600 K.

Commented [CU7]: What happens between 479 and 485 K? What is the magnetic state of the sample in that temperature range?

Arrott plots for the reverse ST and MT, as shown in Fig. 3(c) and (d), were obtained by plotting the values of $M(\mu_o H)$ and $\mu_o H$ as a function of M^2 versus $\mu_o H/M$ [26, 27]. As confirmed in Refs. [28, 29], the phase transition order may be judged by the shape of low-field Arrott plots near phase transition temperature. From Fig. 3(c), the ST is of first-order type as the plots at temperature ranging from 371 to 431 K exhibit S shape. From Fig. 3(d), the MT is of second-order type as the plots display linear behaviour.

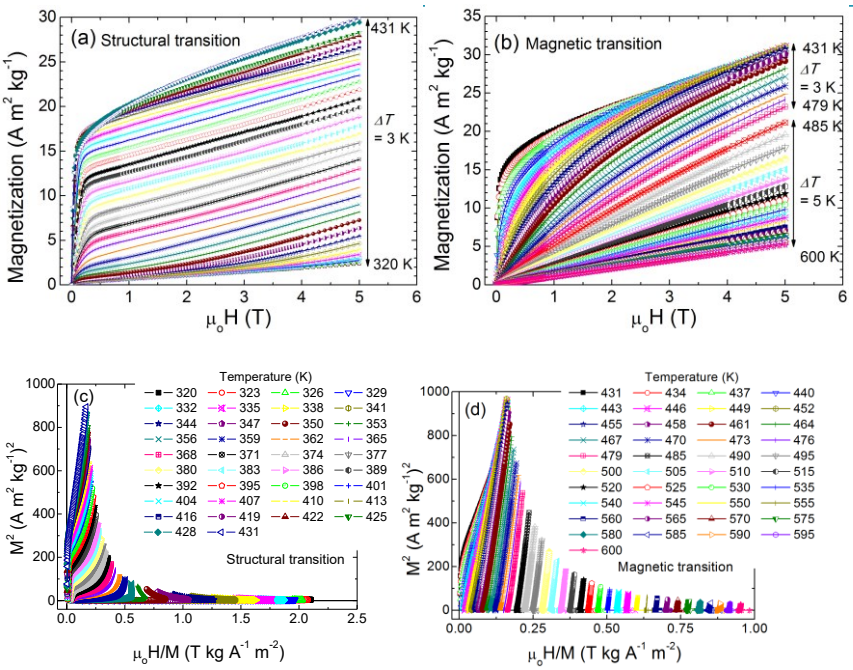

Fig. 3 Isothermal magnetization curves (a, b) and Arrott plots (c, d) around the reverse ST and MT.

We calculated the ΔS_M using the Maxwell relation (i.e., $\Delta S_M(T,\mu_0 H) = \mu_0 \int_0^{\mu_0 H} \left[\frac{\partial M(T,\mu_0 H')}{\partial T}\right]_{\mu_0 H'} dH'$) and plotted its dependence on temperature and magnetic field change in Fig. 4. The ΔS_M^{peak} is nearly the same for both the ST and MT below a value of 2 J kg^{-1} K^{-1} under 5 T field change. This can be attributed to the low $\Delta M_{A\text{-}M}$ within a wide temperature interval of the reverse ST and the formation of second phase. Although this value is considerably lower than other Ni-Mn based Heusler alloys, the δT_{FWHM} for the ST and MT is extended to 66 K and 52 K, respectively under 5 T field. Thus, the total working temperature window reaches 118 K. As confirmed in our previous work [10], a broad working temperature window can be attained by introducing chemical segregation using the directional solidification. The present results imply

that, the working temperature windows of both transitions (ST and MT) are considerably enlarged in directionally solidified polycrystals.

Such large values of δT_{FWHM} suggest that a high *RC* may be achieved even though the present ΔS_M is relatively small, since *RC* is the product of ΔS_M^{peak} and δT_{FWHM}. [30]. The dependences of *RC* on the magnetic field change for the structural and magnetic transitions are present in Fig. 5. The *RC* shows a linear increasing tendency with the increase of field. For $\mu_o\Delta H$ = 5 T, the maximum *RC* reaches high values of 118 and 95 J kg^{-1} for the ST and MT, respectively. They are larger than those reported in $Ni_{50}Mn_{37}Sb_{13}$ (ΔS_M^{peak} = 9.1 J kg^{-1} K^{-1}, *RC* = 37.7 J kg^{-1}) [22], $Ni_{50}Mn_{37}Sn_{13}$ (ΔS_M^{peak} = 22 J kg^{-1} K^{-1}, *RC* = 75 J kg^{-1}) [31], $Ni_{43}Mn_{40}Sn_{10}Cu_7$ (ΔS_M^{peak} = 9.0 J kg^{-1} K^{-1}, *RC* = 35 J kg^{-1}) [32], and $Ni_{52}Mn_{26}Ga_{22}$ (ΔS_M^{peak} = 30 J kg^{-1} K^{-1}, *RC* = 75 J kg^{-1}) [33]. It is indicated that, to attain a large *RC* in the magnetic refrigerants, enlarging the δT_{FWHM} is a good way. This method also provides a wide working temperature window.

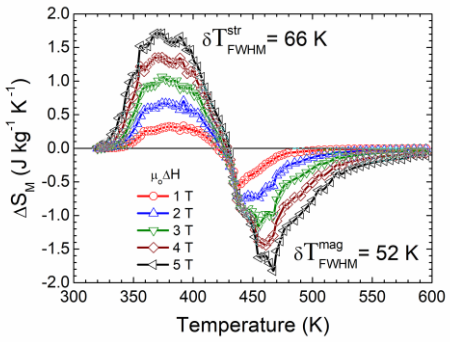

Fig. 4 $\Delta S_M(T)$ curves across the structural and magnetic transitions for five selected $\mu_o\Delta H$ values.

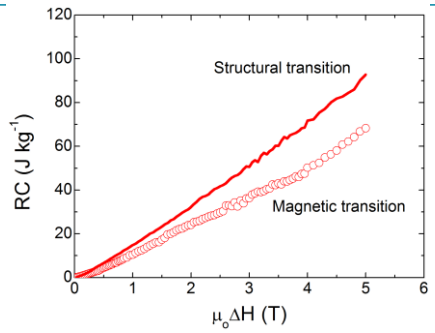

Fig. 5 Refrigeration capacity as a function of the magnetic field change for the structural and magnetic transitions.

4 Conclusions

In summary, we reported the wide structural and magnetic successive transitions in a directionally solidified $Ni_{45}Co_{6.4}Mn_{37}In_{11.6}$ alloy. XRD and SEM studies demonstrate that the microstructure is dual-phase consisting of precipitates of a second phase within a tetragonal martensite matrix. Under 5 T field, the δT_{FWHM} for the ST and MT is extended to 66 K and 52 K, respectively, even combined with a considerably small magnetic entropy change = 2 J kg^{-1} K^{-1}, large values of refrigerant capacity (118 J kg^{-1} for the ST and 95 J kg^{-1} for the MT) are achieved. Enlarging the δT_{FWHM} is a good way to attain a large *RC* in the magnetic refrigerants. Enlarging the δT_{FWHM} also provides a wide working temperature window.

Acknowledgment

The Fundamental Research Funds for the Central Universities (HEUCFG201836) and the State Scholarship Fund of China supported this work. PM acknowledges financial support through the National Science Foundation through grant No DMR-1710640. J.L. Sánchez Llamazares acknowledges the support received from Laboratorio Nacional de Investigaciones en Nanociencias y Nanotecnología (LINAN, IPICyT). C.F. Sánchez-Valdés thanks División Multidisciplinaria in Ciudad Universitaria for financial support.

References

[1] P.J. Brown, A.P. Gandy, K. Ishida, R. Kainuma, T. Kanomata, K.U. Neumann, K. Oikawa, B. Ouladdiaf, K.R.A. Ziebeck, J. Phys.: Condens. Matter 18 (2006) 2249-2259.
[2] J. Liu, N. Scheerbaum, J. Lyubina, O. Gutfleisch, Appl. Phys. Lett. 93 (2008) 102512.
[3] J. Liu, T.G. Woodcock, N. Scheerbaum, O. Gutfleisch, Acta Materialia 57 (2009) 4911-4920.
[4] D. Bourgault, J. Tillier, P. Courtois, D. Maillard, X. Chaud, Appl. Phys. Lett. 96 (2010) 132501.
[5] T. Gottschall, K.P. Skokov, B. Frincu, O. Gutfleisch, Appl. Phys. Lett. 106 (2015) 021901.
[6] F. Cheng, L. Gao, Y. Wang, J. Wang, X. Liao, S. Yang, J. Magn. Magn. Mater. 478 (2019) 234-238.
[7] A.M. Tishin, Y.I. Spichkin, The magnetocaloric effect and its applications, Institute of Physics, 2003.
[8] A. Chaturvedi, S. Stefanoski, M.H. Phan, G.S. Nolas, H. Srikanth, Appl. Phys. Lett. 99 (2011) 162513.
[9] H.C. Tian, X.C. Zhong, Z.W. Liu, Z.G. Zheng, J.X. Min, Mater. Lett. 138 (2015) 64-66.
[10] F. Chen, Y.X. Tong, L. Li, J.L. Sánchez Llamazares, C.F. Sánchez-Valdés, P. Müllner, J. Alloys Compd. 727 (2017) 603-609.
[11] T. Krenke, M. Acet, E. Wassermann, X. Moya, L. Mañosa, A. Planes, Physical Review B 72 (2005) 014412.
[12] M. Pötschke, U. Gaitzsch, S. Roth, B. Rellinghaus, L. Schultz, J. Magn. Magn. Mater. 316 (2007) 383-385.
[13] P.Q. Zheng, N.J. Kucza, Z.L. Wang, P. Müllner, D.C. Dunand, Acta Mater. 86 (2015) 95-101.
[14] G. Uwe, C. Robert, W. Linda, B. Andrea, S. Werner, O. Carl - Georg, B. Heinz - Günter, L. Thomas, N. Iñaki, P. Martin, Advanced Engineering Materials 14 (2012) 636-652.
[15] F. Chen, W.L. Liu, Y.G. Shi, P. Müllner, J. Magn. Magn. Mater. 377 (2015) 137-141.
[16] F. Chen, Y.X. Tong, Y.J. Huang, B. Tian, L. Li, Y.F. Zheng, Intermetallics 36 (2013) 81-85.
[17] Z. Wu, Z. Liu, H. Yang, Y. Liu, G. Wu, R.C. Woodward, Intermetallics 19 (2011) 445-452.
[18] E. Villa, E. Villa, M. Melzi D'Eril, A. Nespoli, F. Passaretti, J. Alloys Compd. 763 (2018) 883-890.
[19] S.Y. Yu, Z.X. Cao, L. Ma, G.D. Liu, J.L. Chen, G.H. Wu, B. Zhang, X.X. Zhang, Appl. Phys. Lett. 91 (2007) 102507.
[20] W. Ito, X. Xu, R.Y. Umetsu, T. Kanomata, K. Ishida, R. Kainuma, Appl. Phys. Lett. 97 (2010) 242512.
[21] R. Kainuma, Y. Imano, W. Ito, Y. Sutou, H. Morito, S. Okamoto, O. Kitakami, K. Oikawa, A. Fujita, T. Kanomata, K. Ishida, Nature 439 (2006) 957-960.
[22] J. Du, Q. Zheng, W.J. Ren, W.J. Feng, X.G. Liu, Z.D. Zhang, J. Phys. D: Appl. Phys. 40 (2007) 5523-5526.
[23] T. Krenke, E. Duman, M. Acet, E. Wassermann, X. Moya, L. Mañosa, A. Planes, E. Suard, B. Ouladdiaf, Phys. Rev. B 75 (2007).
[24] Z.D. Han, D.H. Wang, B. Qian, J.F. Feng, X.F. Jiang, Y.W. Du, Jpn. J. Appl. Phys. 49 (2010) 010211.
[25] J. Liu, T. Gottschall, K.P. Skokov, J.D. Moore, O. Gutfleisch, Nat. Mater. 11 (2012) 620-626.
[26] A. Arrott, Physical Review 108 (1957) 1394.
[27] K.U. Neumann, K.R.A. Ziebeck, J. Magn. Magn. Mater. 140-144 (1995) 967-968.
[28] D.H. Wang, S.L. Tang, S.L. Huang, J.R. Zhang, Y.W. Du, J. Magn. Magn. Mater. 268 (2004) 70-74.
[29] Q.Y. Dong, J. Chen, J. Shen, J.R. Sun, B.G. Shen, J. Magn. Magn. Mater. 324 (2012) 2676-2678.
[30] A.M. Tishin, Y.I. Spichkin, The magnetocaloric effect and its applications, Institute of Physics Publishing, Bristol, 2003.
[31] T.L. Phan, P. Zhang, N.H. Dan, N.H. Yen, P.T. Thanh, T.D. Thanh, M.H. Phan, S.C. Yu, Appl. Phys. Lett. 101 (2012) 212403.
[32] P.O. Castillo-Villa, L.s. Mañosa, A. Planes, D.E. Soto-Parra, J.L. Sánchez-Llamazares, H. Flores-Zúñiga, C. Frontera, J. Appl. Phys. 113 (2013) 053506.
[33] Z. Li, Y. Zhang, C.F. Sánchez-Valdés, J.L. Sánchez Llamazares, C. Esling, X. Zhao, L. Zuo, Appl. Phys. Lett. 104 (2014) 044101.